A panel of embryonic stem cell lines reveals the variety and dynamic of pluripotent states in rabbits

Pierre Osteil, Anaïs Moulin, Claire Santamaria, Thierry Joly, Luc Jouneau, Maxime Aubry, Yann Tapponnier, Catherine Archilla, Barbara Schmaltz-Panneau, Jerôme Lecardonnel, et al.

Stem Cell Reports
Article

OPEN ACCESS

A Panel of Embryonic Stem Cell Lines Reveals the Variety and Dynamic of Pluripotent States in Rabbits

Pierre Osteil,[1,2,3] Anaïs Moulin,[1] Claire Santamaria,[1] Thierry Joly,[4,5] Luc Jouneau,[6] Maxime Aubry,[1] Yann Tapponnier,[1] Catherine Archilla,[6] Barbara Schmaltz-Panneau,[6] Jérôme Lecardonnel,[7] Harmonie Barasc,[8,9] Nathalie Mouney-Bonnet,[8,9] Clémence Genthon,[10] Alain Roulet,[10] Cécile Donnadieu,[10] Hervé Acloque,[10] Elen Gocza,[11] Véronique Duranthon,[6] Marielle Afanassieff,[1,2,*] and Pierre Savatier[1,*]

[1]Univ Lyon, Université Lyon 1, INSERM, Stem Cell and Brain Research Institute U1208, 69500 Bron, France
[2]INRA, USC1361, 69500 Bron, France
[3]Embryology Unit, Children's Medical Research Institute, CMRI, Westmead, NSW 2145, Australia
[4]ISARA-Lyon, 69007 Lyon, France
[5]VetAgroSup, UPSP ICE, 69280 Marcy l'Etoile, France
[6]UMR BDR, INRA, ENVA
[7]GABI, INRA, AgroParisTech
Université Paris-Saclay, 78350 Jouy-en-Josas, France
[8]INRA, UMR 444, Génétique Cellulaire, 31076 Toulouse, France
[9]ENVT, 31076 Toulouse, France
[10]INRA, UMR1388 Génétique, Physiologie et Systèmes d'Elevage, 31326 Castanet Tolosan, France
[11]NARIC, Agricultural Biotechnology Institute, 2100 Gödöllo, Hungary
*Correspondence: marielle.afanassieff@inserm.fr (M.A.), pierre.savatier@inserm.fr (P.S.)
http://dx.doi.org/10.1016/j.stemcr.2016.07.022

SUMMARY

Conventional rabbit embryonic stem cell (ESC) lines are derived from the inner cell mass (ICM) of pre-implantation embryos using methods and culture conditions that are established for primate ESCs. In this study, we explored the capacity of the rabbit ICM to give rise to ESC lines using conditions similar to those utilized to generate naive ESCs in mice. On single-cell dissociation and culture in fibroblast growth factor 2 (FGF2)-free, serum-supplemented medium, rabbit ICMs gave rise to ESC lines lacking the DNA-damage checkpoint in the G_1 phase like mouse ESCs, and with a pluripotency gene expression profile closer to the rabbit ICM/epiblast profiles. These cell lines can be converted to FGF2-dependent ESCs after culture in conventional conditions. They can also colonize the rabbit pre-implantation embryo. These results indicate that rabbit epiblast cells can be coaxed toward different types of pluripotent stem cells and reveal the dynamics of pluripotent states in rabbit ESCs.

INTRODUCTION

Recent advances in exploring the molecular mechanisms of pluripotency revealed major differences between mice and other mammals (Manor et al., 2015; Nichols and Smith, 2009). Mouse embryonic stem cells (ESCs) self-renew in the naive state of pluripotency, a state characterized by permissiveness to single-cell dissociation, inhibiting differentiation by interleukin-6 family members, including leukemia inhibitory factor (LIF), stabilizing self-renewal after inhibiting MEK signaling, a transcriptome close to that of the epiblast of the pre- and peri-implantation blastocyst, and the capacity to participate in forming the three germ layers and generate germline chimeras on injection into the blastocelic cavity (Nichols and Smith, 2009). Conversely, ESCs generated from human and monkey pre-implantation embryos self-renew in the primed state of pluripotency as they express lineage markers and appear closer to commitment to differentiation (Nichols and Smith, 2009). The transcriptome of primate ESCs resembles that of EpiSC lines generated from the epiblast of the mouse post-implantation embryo (Brons et al., 2007; Tesar et al., 2007), a pluripotent cell layer that forms before the onset of gastrulation. They also have similar growth requirements. Both primate ESCs and mouse EpiSCs require fibroblast growth factor 2 (FGF2) and transforming growth factor (TGF-β) superfamily factors to inhibit differentiation, and MEK inhibition fails to stabilize self-renewal. Similar to EpiSCs in mice (Tesar et al., 2007), monkey ESCs also did not generate chimeras after an injection in a blastocyst (Tachibana et al., 2012).

Rabbit ESC lines were generated in several laboratories (Honda et al., 2008; Intawicha et al., 2009; Osteil et al., 2013; Tancos et al., 2012; Wang et al., 2006). These lines exhibited the cardinal features of pluripotency including long-term self-renewal, differentiation into ectodermal, mesodermal, and endodermal derivatives, and the capacity to form teratomas after injection into immunocompromised mice. When cytogenetic studies were performed, they featured a normal chromosomal complement (N = 44) (Wang et al., 2006; Osteil et al., 2013). Similar to primate ESCs, rabbit ESCs appear to be inherently primed. They rely on FGF2 and Activin/nodal/TGF-β but not on LIF signaling for the maintenance of pluripotency (Honda et al., 2009; Osteil et al., 2013; Wang et al., 2006, 2008), and express transcription factors associated with primed

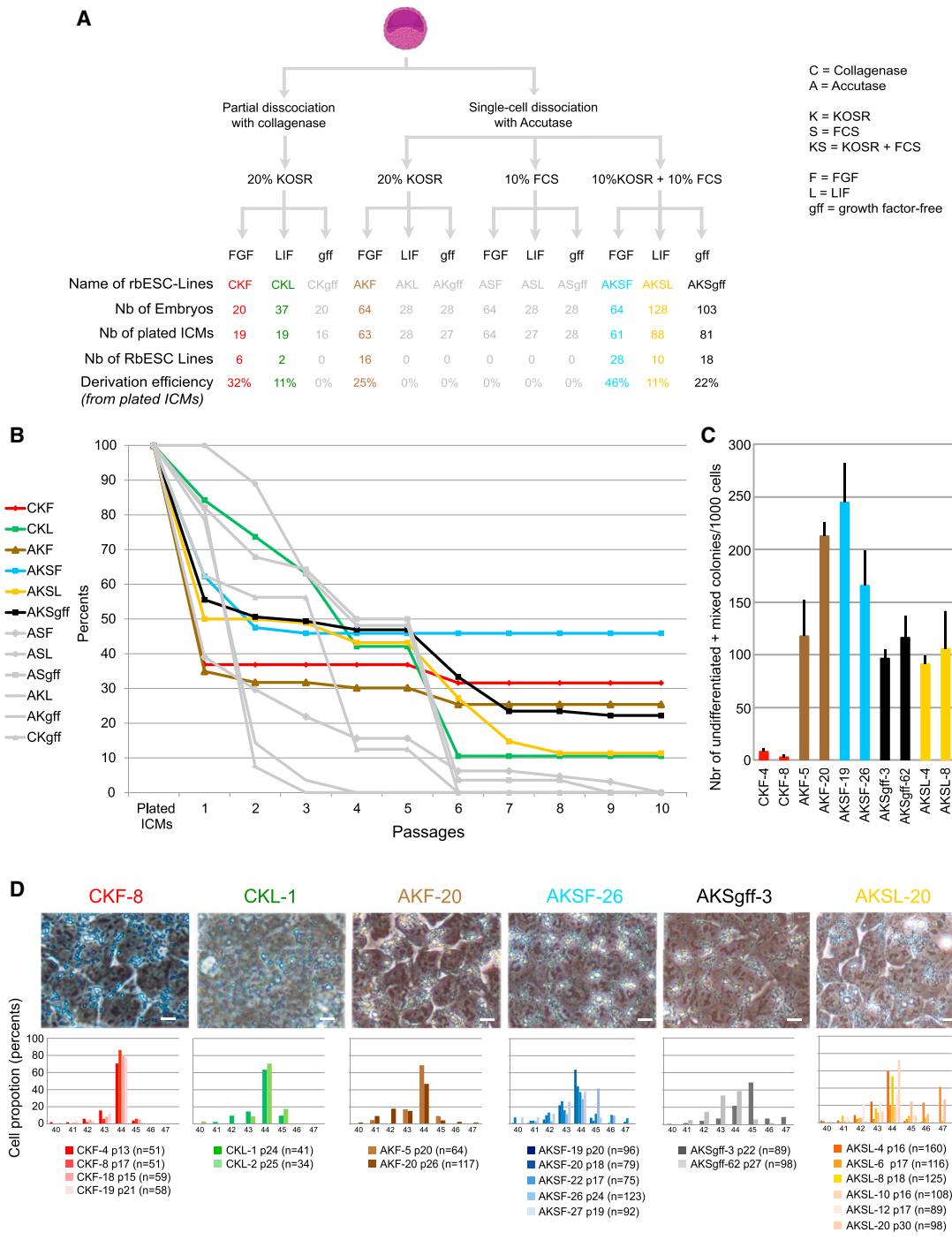

Figure 1. Generation of rbESC Lines

(A) Experimental design.

(B) Percentage of ICMs that survived serial passaging (P1 to P10) in the 12 culture conditions examined (one or two independent experiments depending on conditions).

(C) Number of colonies observed after plating 1,000 cells from CKF-4, CKF-8, AKF-5, AKF-20, AKSF-19, AKSF-26, AKSgff-3, AKFgff-62, AKSL-4, AKSL-8, and AKSL-20 lines (four independent replicates).

(legend continued on next page)

pluripotency in rodents (Osteil et al., 2013; Schmaltz-Panneau et al., 2014). However, we found that rabbit ESCs differ from primate ESCs in two aspects (Osteil et al., 2013). First, they have a different morphology with a lower nuclear-to-cytoplasmic ratio, a characteristic usually associated with a more advanced state in development. Second, they possess a DNA-damage checkpoint in the G_1 phase of the cell cycle, which is absent in mouse, monkey, and human ESCs, and only acquired during differentiation (Aladjem et al., 1998; Filipczyk et al., 2007; Fluckiger et al., 2006; Momcilovic et al., 2009). Whether the presence of the G_1 checkpoint in rabbit ESCs reflects a fundamental difference in pre-implantation embryo development between primates and rabbits or whether rabbit ESCs self-renew even closer to commitment to differentiation than primate ESCs is unknown at this stage. Another key aspect of the biology of rabbit pluripotent stem cells (PSCs) involves induced PSCs (iPSCs). We reported that rabbit iPSCs do not share all defining characteristics of primed pluripotency. Albeit dependent on FGF2 for self-renewal, rabbit iPSCs express naive pluripotency markers at higher levels, the naive-specific distal enhancer of Oct4 is more active, and they can uniquely be propagated using single-cell dissociation with trypsin, unlike rbESCs. Some cells in rabbit iPSC populations can colonize the rabbit pre-implantation embryo (Osteil et al., 2013). Such differences between ESCs and iPSCs have not been described in mice and primates.

We aimed to explore the capacity of the rabbit inner cell mass (ICM) to produce ESCs using culture conditions (dissociation method and growth factor supplementation) similar to those utilized to generate naive ESCs in mice. We analyzed the cell-cycle, transcriptome, and signaling pathways of the so-called AKF, AKSF, AKSL, and AKSgff lines. We also assessed their ability to colonize the rabbit epiblast after injection into pre-implantation embryos.

RESULTS

Derivation of Rabbit ESC Lines Using Different Culture Conditions

In rabbits, embryos reach the 8-cell stage, 32-cell stage, and morula at approximately 36, 48, and 60 hr post coitum (hpc), respectively (Püschel and Viebahn, 2010). Cavitation starts at approximately 80 hpc (early blastocyst, embryonic day 3.5 [E3.5]). The mid-blastocyst stage is reached at approximately 96 hpc (E4), and the late blastocyst is first observed at 120 hpc (E5). The expanded blastocyst stage is reached at approximately 140 hpc (E6).

We aimed to derive rbESC lines from E4 mid-blastocysts, employing methods and culture conditions used to generate mESCs. At first we tried to derive ESC lines using MEK and GSK3β inhibitors in DMEM/F12 or neurobasal N2B27 medium (2i/LIF condition), a condition used to derive mESC lines from non-permissive mouse strains (Ying et al., 2008). However, no line could be obtained from rabbit blastocysts (Figure S1). We then opted for the following strategy: 612 E4 embryos were microdissected to isolate the ICM. ICMs were subsequently plated onto growth-inactivated murine embryonic fibroblasts (MEFs). Three key parameters were tested, resulting in 12 different conditions: (1) dissociation method (single-cell dissociation with Accutase [A] or partial dissociation with collagenase II [C]); (2) serum supplementation (20% KnockOut Serum Replacement [KOSR] [K], 10% KOSR + 10% fetal calf serum [FCS] [KS], or 10% FCS [S]); and (3) growth factors (FGF2 [F], LIF [L], or growth factor-free [gff]) (Figure 1A). All cell lines that survived beyond passage 10 after dissociating the primary outgrowth sustained long-term culture. Thus, derivation was considered successful if cell lines could be cultured beyond passage 10. Of the 12 aforementioned conditions, only six gave rise to rbESC lines (Figures 1A and 1B): (1) six lines (32% of embryos) were generated using collagenase II + 20% KOSR + FGF2 (CKF condition); (2) two lines (11% of plated ICMs) were generated using collagenase II + 20% KOSR + LIF (CKL condition); (3) 16 lines (25% of embryos) were generated using Accutase + 20% KOSR + FGF2 (AKF condition); (4) 28 lines (46% of embryos) were generated using Accutase + 10% KOSR + 10% FCS + FGF2 (AKSF condition); (5) ten lines (11% of plated ICMs) were generated using Accutase + 10% KOSR + 10% FCS + LIF (AKSL condition); and (6) 18 lines (22% of plated ICMs) were generated using Accutase + 10% KOSR + 10% FCS without FGF2 or LIF (gff condition; AKSgff). Thus, KOSR appeared essential to derivation, as no rbESCs could be generated in medium supplemented with FCS alone regardless of the dissociation method and growth factor supplementation. The efficiency of derivation varied dramatically among the six conditions. The highest efficiency was observed with FGF2 (AKSF, CKF, and AKF), followed by lack of growth factor (AKSgff), and the lowest was with LIF (AKSL and CKL), regardless of the dissociation protocol used for cell passaging.

Overall, 11 of 80 lines were subjected to a colony-forming assay to evaluate cloning efficiency. All cell lines

(D) Phase-contrast images for CKF-8, CKL-1, AKF-20, AKSF-26, AKSgff-3, and AKSL-20 lines. Histograms show the distribution of chromosome numbers in 21 ESC lines at the indicated passages (n indicates the number of metaphases analyzed for each line from one experiment). Scale bars, 10 μm.
See also Figures S1–S3.

generated and propagated with Accutase (AKF, AKSF, AKSgff, and AKSL) generated 17 (AKSL-4) to 61 (AKSL-8) times more colonies than the CKF lines (Figure 1C). Overall, 21 of 80 lines generated were subjected to chromosomal counting. Ten lines exhibited a normal chromosomal complement (N = 44). Three lines (AKSL-6, AKSL-10, and AKSgff-3) displayed a supplementary chromosome in 20%–50% of cells, suggesting that single-cell dissociation combined with culture in FGF2-null medium resulted in increased genetic instability (Figure 1D). Colony morphology differed between groups. CKL, AKSF, and AKSgff colonies contained tightly packed cells, whereas those of CKF, AKF, and AKSL featured larger cells (Figures 1D and S2A). One cell line from each of the six groups (CKF-8, CKL-1, AKF-20, AKSF-26, AKSL-20, and AKSgff-3) was tested for its capacity to form teratomas after injection under the kidney capsule of immunodeficient mice. Teratomas comprising differentiated cells representative of the three germ layers were obtained from all six lines (Figure S2B). All six lines also expressed the pluripotency-specific transcription factor Oct4 in virtually all cells (Figure S3A). However, the percentage of cells expressing stage-specific embryonic antigen (SSEA)-1 and -4 varied extensively between lines, ranging from 2% (AKF-20) to 64% (AKSF-26) for SSEA1, and from 3% (AKSgff-62) to 75% (AKSF-26) for SSEA4 (Figures S3B–S3D). It is unlikely that the SSEA-negative cells are differentiated, as most cells in the populations were positive for Oct4. Moreover, we previously showed that the SSEA1$^+$, SSEA4$^+$, and SSEA$^-$ rabbit iPSCs were capable of interconversion in culture, strongly suggesting that they represent metastable states (Osteil et al., 2013). To conclude, the culture conditions applied to ICM outgrowths and rbESCs altered several cell parameters, including colony morphology, cloning efficiency, genome stability, and the frequency of SSEA1$^+$ and SSEA4$^+$ cells.

Cell-Cycle Parameters Are Altered by Serum and Growth Factor Supplementation

A total of 12 cell lines were analyzed for cell-cycle parameters: nine lines (CKF-4, CKF-8, CKL-1, AKF-5, AKF-20, AKSL-4, AKSL-8, AKSL-20, and AKSF-19) displayed a majority (55%–85%) of euploid cells; three lines (AKSgff-3, AKSgff-62, and AKSF-26) displayed heterogeneous karyotypes with 20%–40% of euploid cells. Differences in cell growth were observed between rbESC lines. AKSgff cell lines displayed a lower growth rate (doubling time 41.3 ± 9.5 hr) than AKSF, AKF, and AKSL cell lines (doubling time 25.8 ± 2.0, 24.7 ± 0.6, and 20.5 ± 0.1 hr, respectively, Figure 2A). Differences in cell-cycle distribution were also observed. In particular, the proportion of cells in the G_1 and G_2 phases of the cell cycle considerably varied between lines (ranging from 23% to 71% for G_1 and from 16% to 54% for G_2) (Figures 2B and S4A). A similar heterogeneity in cell-cycle distribution was observed in the SSEA1$^+$ cell fraction, excluding the possibility that these variations reflect spontaneous differentiation. However, a consistent pattern was also observed showing a smaller G_1 fraction and a larger G_2 fraction in the SEEA1$^+$ cells compared with the SSEA1$^-$ cells (Figures 2B and S4B).

Both rodent and primate PSCs have an altered response to DNA-damaging agents. They lack a DNA-damage checkpoint in the G_1 phase (Aladjem et al., 1998; Filipczyk et al., 2007; Fluckiger et al., 2006; Momcilovic et al., 2009). Rabbit ESC lines also displayed remarkable differences. No accumulation of 2N cells was observed in AKF, AKSF, AKSL, and AKSgff lines after treatment with the DNA-damaging agent doxorubicin for 24 hr, indicating the lack of a DNA-damage checkpoint in the G_1 phase (Figure 2C). Conversely, all CKF and CKL lines exhibited accumulation of doxorubicin-treated cells with both 2N and 4N DNA content, indicating DNA-damage checkpoints in both the G_1 and G_2 phases as in somatic cells. These results suggest that single-cell dissociation with Accutase erases the G_1 DNA-damage checkpoint that characterizes differentiated cells.

Transcriptome Reconfiguration Induced by Cell Dissociation and Growth Factor Supplementation

We used rabbit-specific gene expression microarray (Jacquier et al., 2015) to analyze the expression of approximately 13,000 genes in CKF-4, CKF-8, AKF-5, AKF-20, AKSL-4, AKSL-8, AKSL-20, AKSF-19, AKSF-26, AKSgff-3, and AKSgff-62 (Gene Ontology accession number GEO: GSE79195). Given the inherent instability of CKL cells, they were not included in the transcriptome analysis. The gene expression profiles of the 11 aforementioned cell lines were compared with those of the ICM (mid-blastocyst, E4) and epiblast (expanded blastocyst, E6). Hierarchical clustering of normalized data (39 samples) resulted in three large clusters (Figure 3A): (1) E4-stage ICM and E6-stage epiblast; (2) rbESCs lines derived and propagated after partial dissociation with collagenase (CKF); and (3) rbESCs lines derived and propagated after single-cell dissociation with Accutase (AKF, AKSF, AKSL, and AKSgff). Thus, in vitro culture and dissociation methods were the two main sources of difference among the 39 samples analyzed. The third cluster, comprising 27 samples, is subdivided into two smaller clusters containing all cell lines derived in the absence (FGF$^-$) and presence (FGF$^+$) of FGF2 supplementation, respectively. To investigate this latter partition further, we built a PLS-DA model using the ropls package (Thevenot et al., 2015) (Figure 3B). This analysis identifies two directions in space segregating "FGF$^+$" and "FGF$^-$" samples. R2Y and Q2Y are PLS-DA metrics allowing the estimation of the accuracy of the model. We see that we have

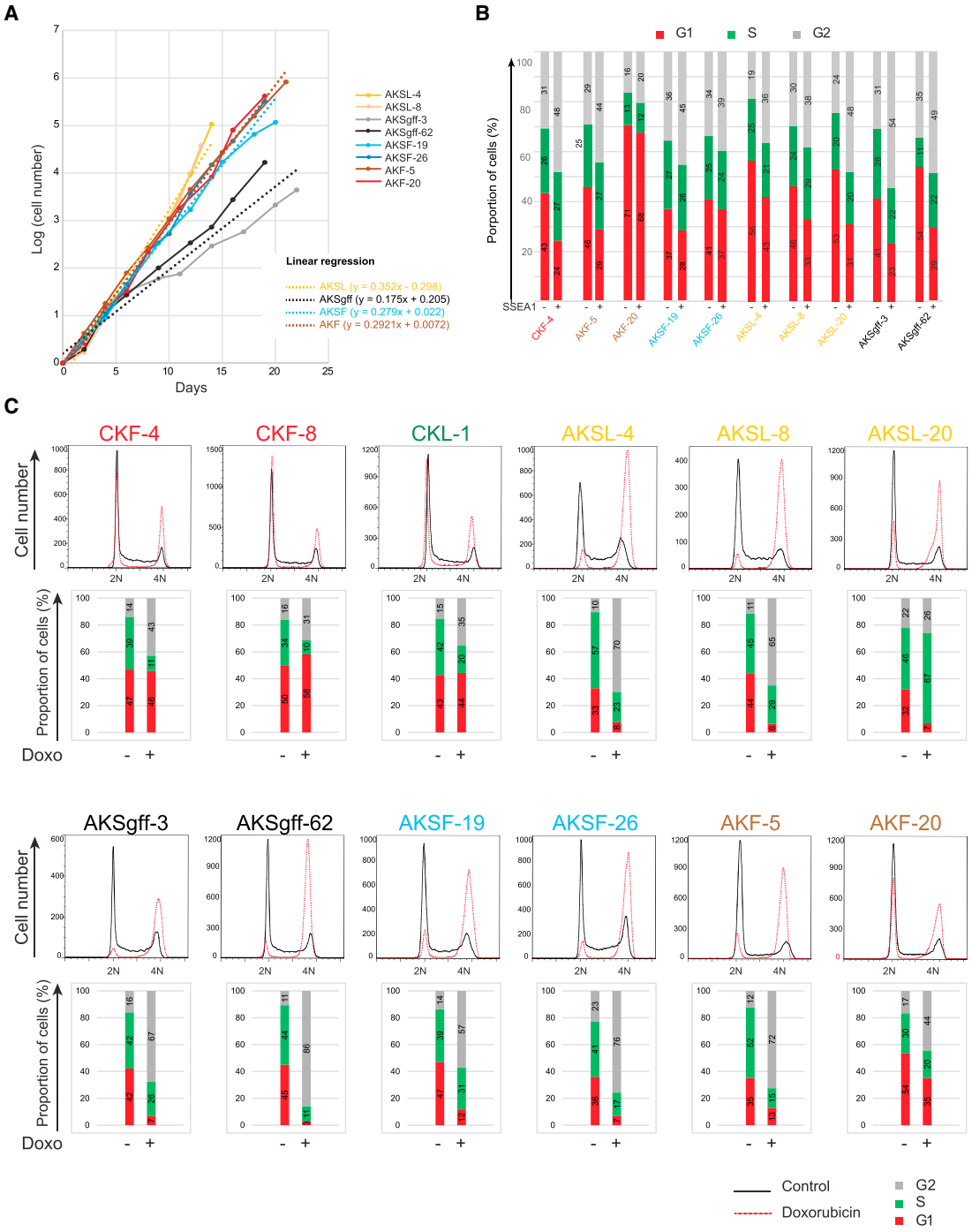

Figure 2. Cell-Cycle Analysis

(A) Growth curves for AKF, AKSF, AKSL, and AKSgff cells. The dotted lines represent the linear regression, the coefficients of which (slope and intercept) were calculated by the least-squares method for each cell line.

(B) Histograms showing the percentages of G_1-, S-, and G_2/M-phase cells in both SSEA1-negative and SSEA1-positive cell populations after staining with propidium iodide, calculated using FlowJo software (the results of one representative of two independent experiments are shown).

(C) Cell-cycle profiles for the 12 cell lines before and after doxorubicin treatment. Histograms show the percentages of G_1-, S-, and G_2/M-phase cells before and after doxorubicin treatment calculated using FlowJo software.

See also Figure S4.

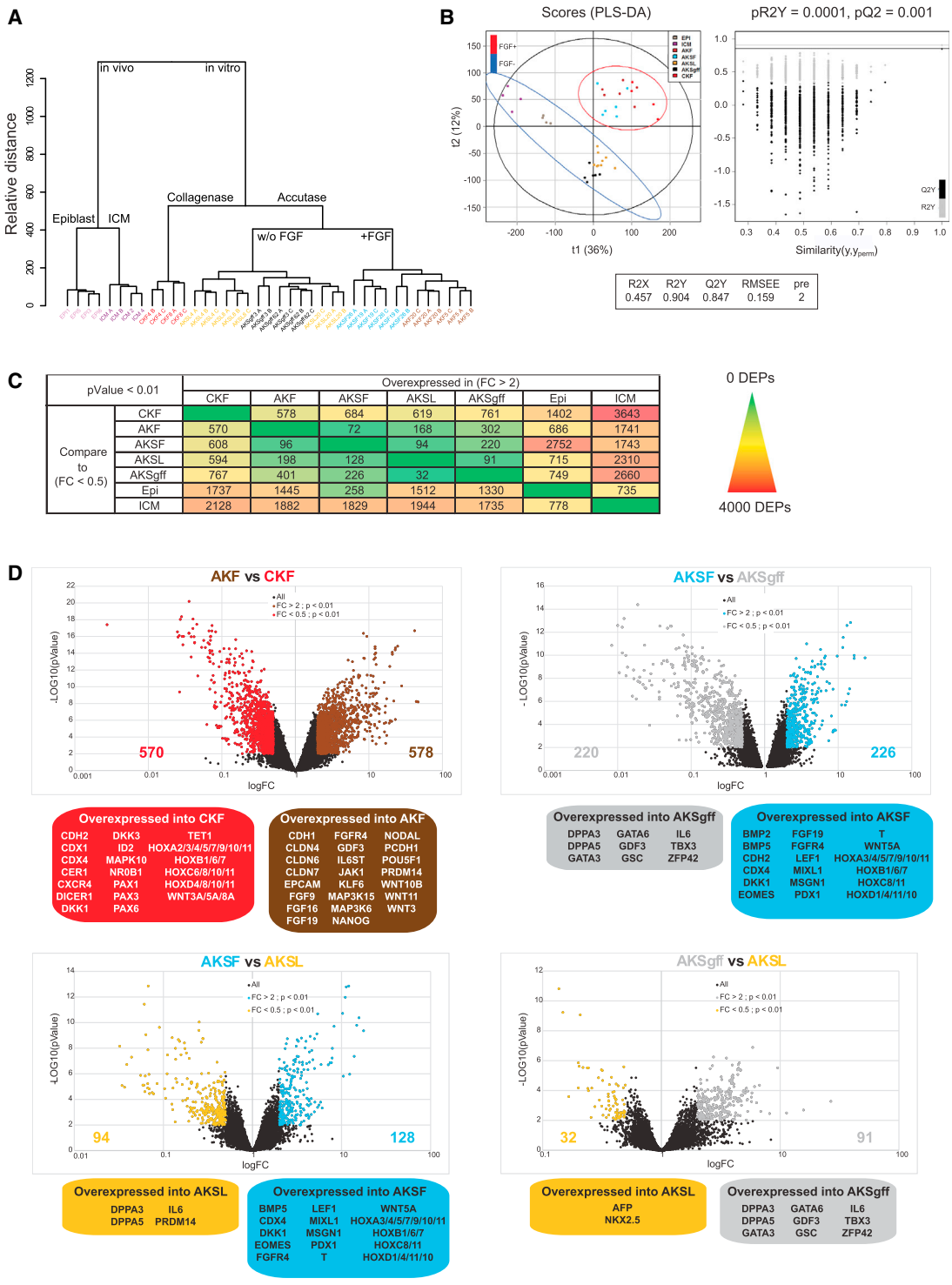

Figure 3. Transcriptome Analysis

(A) Hierarchical clustering of whole-transcriptome data of all cell types (three to four independent replicates per cell type) using Pearson's correlation coefficient as a measure of the distance between the samples.

(B) Statistical evaluation of the partition between FGF^{-} and FGF^{+} samples. Left panel: projection of individual X-score values on the two components identified by PLS-DA analysis. Right panel: R2 and Q2 values after permutation of sample's condition. The horizontal gray and black lines indicate the values of R2 and Q2 obtained with observed data (i.e., without permutations), respectively.

(legend continued on next page)

high values for R2Y and Q2Y (these two metrics have values in the range of [0; 1]). Moreover, whatever the substitution is made between the two classes of the samples, we cannot find a better model than the one we initially proposed (all R2 and Q2 metrics obtained after substitution have a lower value than the one obtained with the initial classification: gray line for R2 and black line for Q2). This indicates that our model is robust and is not subject to overfitting. Therefore, FGF2 is a third source of difference among the samples analyzed. Together, these results indicate that both the dissociation method and growth factor supplementation applied to ICM outgrowth and all subsequent cultures dramatically influence the transcriptome of the resulting rbESC lines. It must be stressed that the transcriptome of ESC lines containing aneuploid cells did not differ from that of their euploid counterparts derived and propagated in the same culture regime. The same conclusion could be reached on the basis of the cell-cycle parameters. This suggests that the impact of genetic changes is low with regard to the sensitivity of the methods used to characterize the ESC lines.

To obtain further insights into the genes up- and downregulated between different cell lines and embryo samples, we extracted the differentially expressed probe sets (adjusted p value <0.01; fold change <0.5 or >2) from the compendium and annotated them according to the Ensembl Ocu database (Ensembl Genes 75, OryCun2.0). The two most divergent samples were ICM and CKF cells (5,771 differentially expressed probe sets), and the two closest were AKSL and AKSgff (123 differentially expressed probe sets) (Figure 3C). Pairwise comparison revealed that the pluripotency genes *Pou5f1* (*Oct4*), *Nanog*, and *Prdm14*, the LIF signaling genes *Il6st* (*gp130*) and *Jak1*, and *FGF* and *Clnd6* genes were upregulated in AKF cells compared with CKF cells (Figure 3D and Table S1). Conversely, *Hox* and *Pax* genes were downregulated in AKF cells compared with CKF cells. Thus, in the presence of FGF2, single-cell dissociation reinforced pluripotency gene expression, whereas partial dissociation reinforced lineage-specific gene expression. Pairwise comparison of AKSF to AKSgff or AKSL indicated that the lineage-specific genes *Mixl1*, *T-Bra*, *Eomes*, and *Hox* were upregulated in AKSF cells. Conversely, AKSgff and AKSL cells exhibited higher pluripotency gene expressions of *Dppa3* (*Stella*), *Dppa5*, and *Prdm14* (AKSF versus AKSL) and *Gdf3*, *Tbx3*, and *Rex1* (*Zfp42*) (AKSF versus AKSgff). Thus, FGF2 reinforced lineage-specific gene expression, whereas the absence of FGF2 reinforced pluripotency marker expression. The same pluripotency markers were upregulated in AKSgff cells in a pairwise comparison with AKSL cells, suggesting that LIF negatively affects pluripotency marker expression in AKS cells. These results indicate that partial dissociation with collagenase and FGF2 supplementation activates lineage marker expression in rbESCs, whereas single-cell dissociation with Accutase or a lack of FGF2 supplementation reinforces gene expression associated with the control of pluripotency.

Pluripotency-Associated Genes and miRNAs Discriminate Cell Lines

Whole-transcriptome analysis revealed that *Tbx3*, *Prdm14*, and *Rex1* (*Zfp42*) were differentially expressed among CKF, AKF, AKSF, AKSL, and AKSgff cells. These genes are differentially expressed between the primed and naive states of pluripotency in mice (Bao et al., 2009; Tesar et al., 2007), suggesting that the rabbit ESC lines stand at different positions along the spectrum of pluripotency states. To examine this issue further, we analyzed the expression of 33 genes that are instrumental in discriminating naive and primed pluripotency in rodents (Bao et al., 2009; Tang et al., 2010; Tesar et al., 2007), humans (Chen et al., 2015), and rabbits (Osteil et al., 2013) (*Acta2*, *Bteb2*, *Cer1*, *Cdh1*, *Cdh2*, *Clnd6*, *Dax1* [*NrOb1*], *Dazl*, *Dkk1*, *Dppa2*, *Dppa3*, *Dppa5*, *Eomes*, *Esrrb*, *Fbxo15*, *Foxa2*, *Gata6*, *Gbx2*, *Gdf3*, *Klf4*, *Klf17*, *Myc*, *Nodal*, *Otx2*, *Pitx2*, *Piwil2*, *Rex1* [*Zfp42*], *Sox2*, *Sox17*, *Stra8*, *Tbx3*, *Tet2*, and *Tdgf1*). A heatmap calculated from the microarray data revealed that these genes could efficiently discriminate rbESC lines cultivated with and without FGF2 and rbESC lines undergoing partial dissociation with collagenase as opposed to single-cell dissociation with Accutase (Figure 4A). PCA analysis of the expression of the 33 aforementioned genes clustered the 39 cell lines into four groups: (1) CKF lines, (2) AKF, AKSF, AKSL, and AKSgff lines, (3) epiblast samples, and (4) ICM samples (Figure 4B). Based on this analysis, the rbESC lines propagated in the absence of FGF2 and/or via a protocol involving single-cell dissociation with Accutase displayed a global pluripotency gene expression pattern much closer to that of the epiblast and

(C) Number of differentially expressed probe sets (DEPs) between two lines, ranging from 0 (green) to 4,000 (red).
(D) Volcano plot representation of microarray data. x axis: log fold change (logFC); y axis: −log10(p value). Top left panel: "AKF vs CKF" identifies genes differentially expressed under single-cell dissociation with Accutase compared with partial dissociation with collagenase. Top right panel: "AKSF vs AKSgff" identifies genes differentially expressed with FGF2 supplementation. Bottom left panel: "AKSF vs AKSL" identifies genes differentially expressed with FGF2 supplementation compared with LIF supplementation. Bottom right panel: "AKSgff vs. AKSL" identifies genes differentially expressed with LIF supplementation. Genes of interest are displayed underneath each pairwise comparison.
See also Table S1.

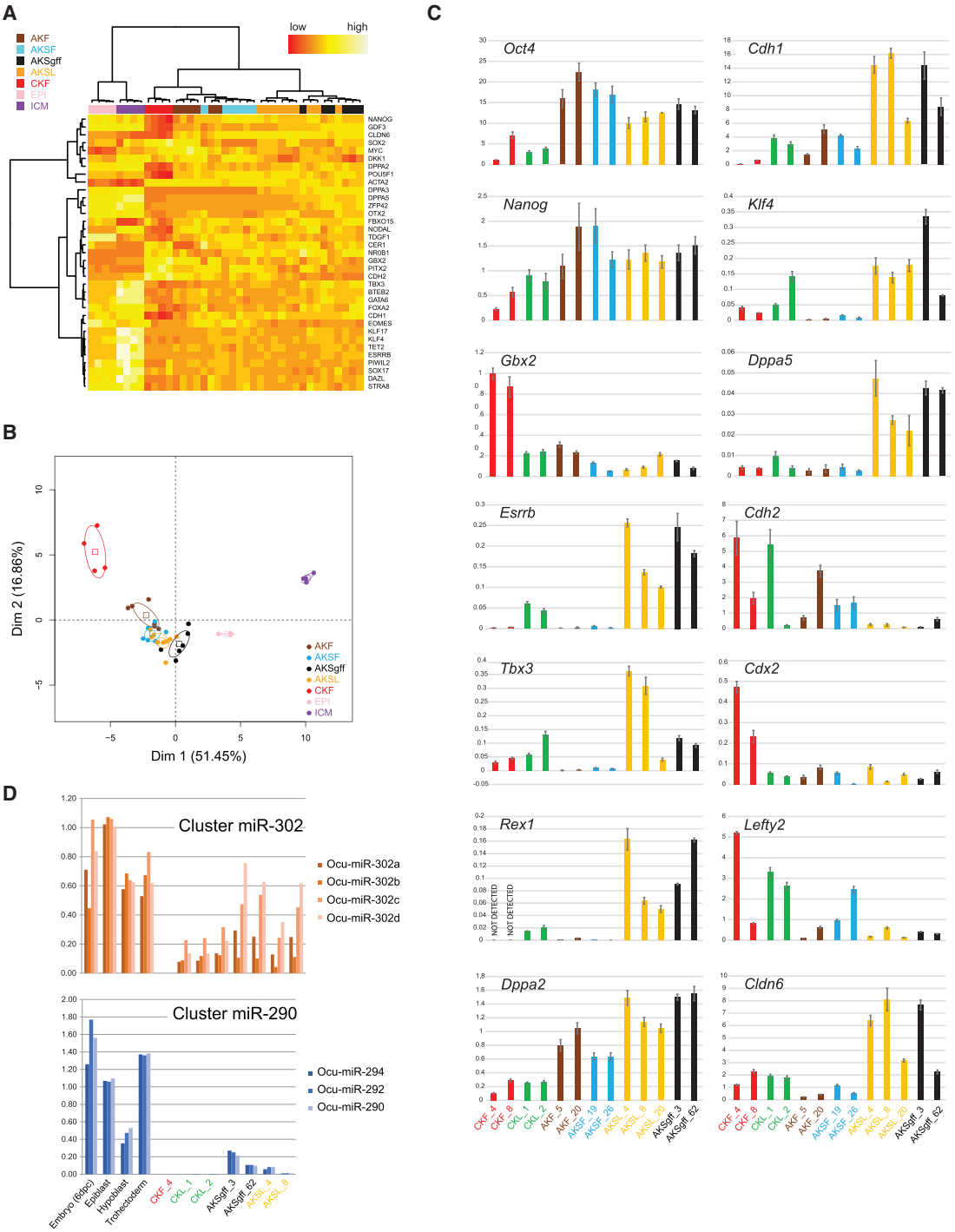

Figure 4. Pluripotency Gene and miRNA Expression Profiling

(A) Heatmap calculated from microarray data. Values displayed correspond to the expression level in each sample adjusted by the mean expression of each gene across samples.

(B) Graphical representation of the two first principal components of PCA for all analyzed samples based on the whole-transcriptome data.

(C) Bar graphs showing the ΔCt values of the 14 pluripotency-associated genes relative to the mRNA level of *Tbp* in CKF, CKL, AKF, AKSF, AKSL, and AKSgff cells (three technical replicates).

(D) Histograms of the expression of pre-implantation embryo-specific *ocu-miR-302* and *ocu-miR-290* clusters relative to the levels of *ocu-miR-191* and *ocu-miR-423* (three technical replicates).

ICM than the conventional CKF lines. AKSL and AKSgff lines clustered closer to epiblast and ICM samples than did AKF lines, suggesting that combining FCS supplementation and FGF2 deprivation resulted in a wider transcriptome reconfiguration. AKSL and AKSgff lines notably expressed *Esrrb*, *Rex1* (*Zfp42*), *Klf4*, and *Cdh1* at higher levels relative to the CKF, CKL, AKF, and AKSF lines (Figure 4C). These four genes are expressed at a higher level in naive PSCs compared with their primed counterpart in rodents (Tesar et al., 2007). AKSL and AKSgff lines also expressed *Cldn6* and *Gbx2* at higher and lower levels, respectively. *Cldn6*, a marker of primed pluripotency in mice, is strongly expressed in the rabbit ICM, whereas *Gbx2*, a marker of naive pluripotency in mice, is weakly expressed in the rabbit ICM (Osteil et al., 2013; Schmaltz-Panneau et al., 2014), revealing differences in the defining markers of naive pluripotency between mice and rabbits. Notably, the pluripotency gene expression profile of ESC lines containing aneuploid cells did not differ from their euploid counterparts derived and propagated using the same culture regime, suggesting that the impact of genetic changes is very low with regard to the sensitivity of the method.

Ocu-miR-294 and *ocu-miR-302* are two miRNA clusters expressed in rabbit pre-implantation embryos. *ocu-miR-294* cluster expression starts at the 1-cell stage and peaks in the ICM of mid-blastocysts (E3.5–E4.5). The *ocu-miR-302* cluster is strongly expressed in the epiblast of early gastrulation embryos (E6–E7) (Maraghechi et al., 2013). We found high *ocu-miR-302* cluster miRNA expressions in all rbESC lines. Importantly, AKSL and AKSgff lines expressed the *ocu-miR-290* cluster members (the rabbit homolog of the naive-state-specific mouse *miR-290* cluster [Parchem et al., 2014]) at higher levels than CKF and CKL lines (Figure 4D). These results suggest that single-cell dissociation and culture in medium lacking FGF2 enrich rbESC populations in cells with an miRNA expression profile closer to that observed in the rabbit ICM.

Alteration of Culture Conditions Reveals Transcriptional Flexibility

Next, we asked whether the observed differences in pluripotency gene expression profiles among the six cell lines resulted from the capture of stable states of pluripotency at the time of outgrowth dissociation, or, alternatively, whether each cell line retained the capacity to change to another type according to culture conditions. This question was addressed by culturing each ESC line for five passages under the five other culture conditions. Note that no rbESC line was expanded under the CKL culture condition (i.e., partial dissociation with collagenase and culture medium supplemented with KOSR and LIF). Our experimental paradigm resulted in 24 new cell lines that were subsequently analyzed for the expression of 25 pluripotency genes using qRT-PCR followed by PCA (Figure 5A) and hierarchical clustering (Figure 5B). We observed that AKF, AKSL, AKSgff, and CKL cell lines acquired a global gene expression profile closer to that of CKF cells after culture in medium supplemented with KOSR and FGF2 and partial dissociation with collagenase. Similarly, CKF, AKSL, AKSgff, and CKL cell lines acquired a global gene expression profile much closer to that of AKF cells after culture in medium supplemented with KOSR and FGF2 and single-cell dissociation with Accutase. More generally, every cell line propagated under any culture condition acquired a global gene expression profile much closer to that of the cell line originally isolated and expanded under this culture condition. Together, these results indicate that the gene expression profile of the six rbESC lines is highly flexible.

Changes in the proportion of G_1 cells were also observed during shifts between culture conditions (Figure 5C). After propagation of AKF, AKSL, AKSgff, and CKL cells in medium supplemented with KOSR + FGF2 and partial dissociation with collagenase (CKF condition), the proportion of G_1 cells increased and in some cases reached the level measured in the original CKF cell line. Similarly, after propagation of CKF and AKF cells in medium supplemented with FCS and single-cell dissociation with Accutase (AKSL and AKSgff conditions), the proportion of G_1 cells decreased to the level measured in the original AKSL and AKSgff cell lines. Thus, G_1 phase duration is influenced by the dissociation method and growth factor supplementation.

Cell Population Heterogeneity

Both AKSgff-62 and AKSL-4 cell lines expressed markers of naive pluripotency at higher levels than any other cell line described in this study. We examined the expression of these markers at the single-cell level to determine whether any cell in the population expresses a full complement of naive markers as defined in mice. The genes examined belonged to four categories: (1) pluripotency genes (*Pou5f1* [*Oct4*] and *Nanog*); (2) genes expressed at a higher level in mESCs compared with EpiSCs (*Esrrb*, *Zfp42* [*Rex1*], *Cdh1*, *Tfcp2l1*, *Tbx3*, *Dax1*, *Klf4*, *Gbx2*, and *FbxO15*); (3) genes expressed at a higher level in EpiSCs compared with mESCs (*Cldn6*, *Cdx2*, *Otx2*, *Lefty2*, and *Pitx2*) (Bao et al., 2009; Brons et al., 2007; Tesar et al., 2007); and (4) genes encoding components of the LIF/STAT3 pathway and its downstream targets (*Il6st* [*gp130*], *Lifr*, *Sp5*, *c-Fos*, *Zfp36*, and *Cyp1b1*) (Bourillot et al., 2009). *Dppa2* and *Dppa5* are expressed at a higher level in rabbit ICM and epiblast compared with rbESCs (Schmaltz-Panneau et al., 2014) and were included in the analysis. Hierarchical clustering of normalized data resulted in two large clusters in both cell lines (Figures 6A

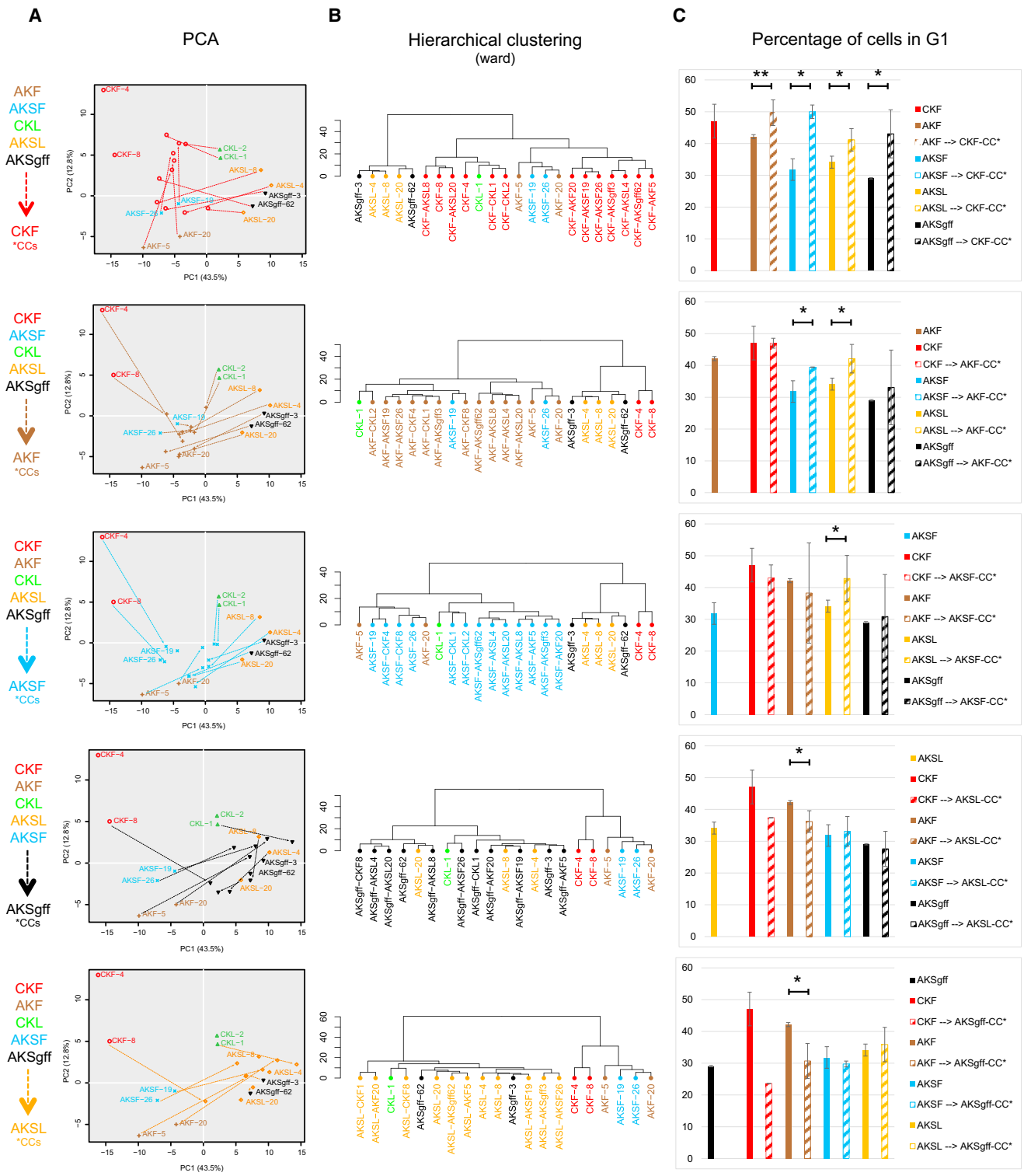

Figure 5. Alteration of Culture Conditions Reveals Transcriptional Flexibility

(A) Graphical representation of the two first principal components of PCA for all analyzed samples (original and adapted cells) based on the expression of 25 pluripotency genes as determined by qRT-PCR (three technical replicates). Arrows indicate the shift in position resulting from new culture conditions for each cell line. The color of the arrows denotes the target cell type; e.g., in the top PCA, red arrows indicate

(legend continued on next page)

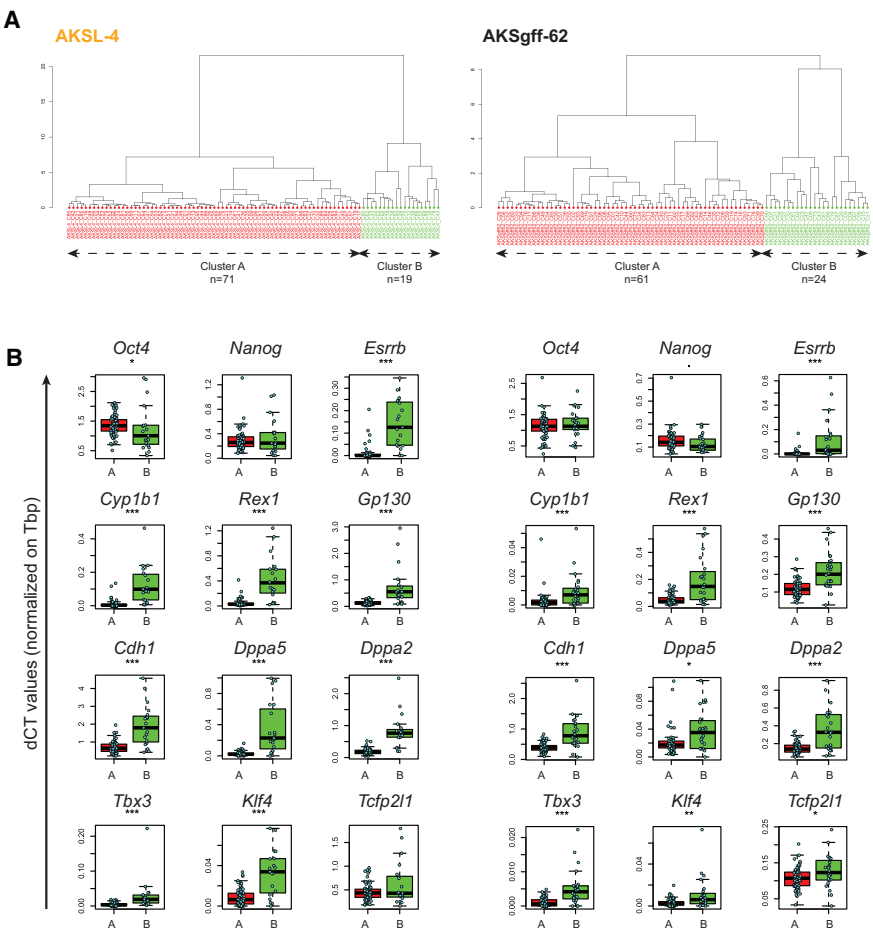

Figure 6. Single-Cell Pluripotency Gene Expression Profiling of AKSL-4 and AKSgff-62 Cells

(A) Hierarchical clustering of qRT-PCR data of all samples (AKSL-4, n = 90 cells; AKSgff-62, n = 85 cells).

(B) Box plots showing the ΔCt values of *Oct4*, *Nanog*, *Esrrb*, *Cyp1b1*, *Rex1*, *gp130*, *Cdh1*, *Dppa5*, *Dppa2*, *Tbx3*, *Klf4*, and *Tfcp2l1* (relative to the mRNA level of *Tbp*). *p < 0.05, **p < 0.01, ***p < 0.001.

See also Figure S5.

and S5). Cluster B represented 21% and 28% of the AKSL-4 and AKSgff-62 populations, respectively. Cells in cluster B expressed *Essrb*, *Dppa2*, *Tbx3*, *Klf4*, *Rex1*, *Dppa5*, and *Tfcp2L1* (AKSgff-62 only) at higher levels than the rest of the cell population (Figure 6B). They also expressed *gp130* and *Cyp1b1*, a target gene of the LIF/STAT3 pathway in mouse ESCs (Bourillot et al., 2009), at higher levels. Together, these results strongly suggest that derivation and propagation of rbESCs using culture medium supplemented with FCS, associated with single-cell dissociation rather than mechanical dissociation, captured some cells with transcriptomic characteristics more similar to those of naive PSCs as defined in mice.

LIF/JAK and Activin Signaling Pathways of AKSL and AKSgff Cells

All cell lines were routinely cultured on growth-inactivated MEFs. Thus, we assessed whether the FGF2-independent AKSL cells were dependent on activin for self-renewal. Removal of feeders and culture on Matrigel resulted in morphological differentiation (Figure S6A), growth arrest after 3 days (Figure 7A), and Nanog and Oct4 downregulation (Figure S6B). These changes were prevented after supplementing AKSL culture medium with either conditioned medium prepared from FGF2-treated MEFs or activin (Figures 7A, S6A, and S6B). Furthermore, treatment of AKSL cells with the activin receptor inhibitor SB431542 for

the shift in position resulting from propagation of CKL-1, CKL-2, AKSL-4, AKSL-8, AKSL-20, AKF-5, AKF-20, AKSF-19, AKSF-26, AKSgff-3, AKSgff-4, and AKSgff-62 cells using the culture conditions for CKF cells (CKF-CCs*).

(B) Hierarchical clustering of qRT-PCR data of all samples described in (A) using Pearson's correlation coefficient as a measure of the distance between the samples. Samples are designated as "target condition–original cell line," e.g., CKF-AKSgff62 denotes AKSgff62 cells that were propagated for five passages using the culture conditions for CKF cells.

(C) Bar graphs showing the percentage of G_1 cells in both original and adapted cell lines, calculated using FlowJo (three independent replicates). *p < 0.05, **p < 0.01.

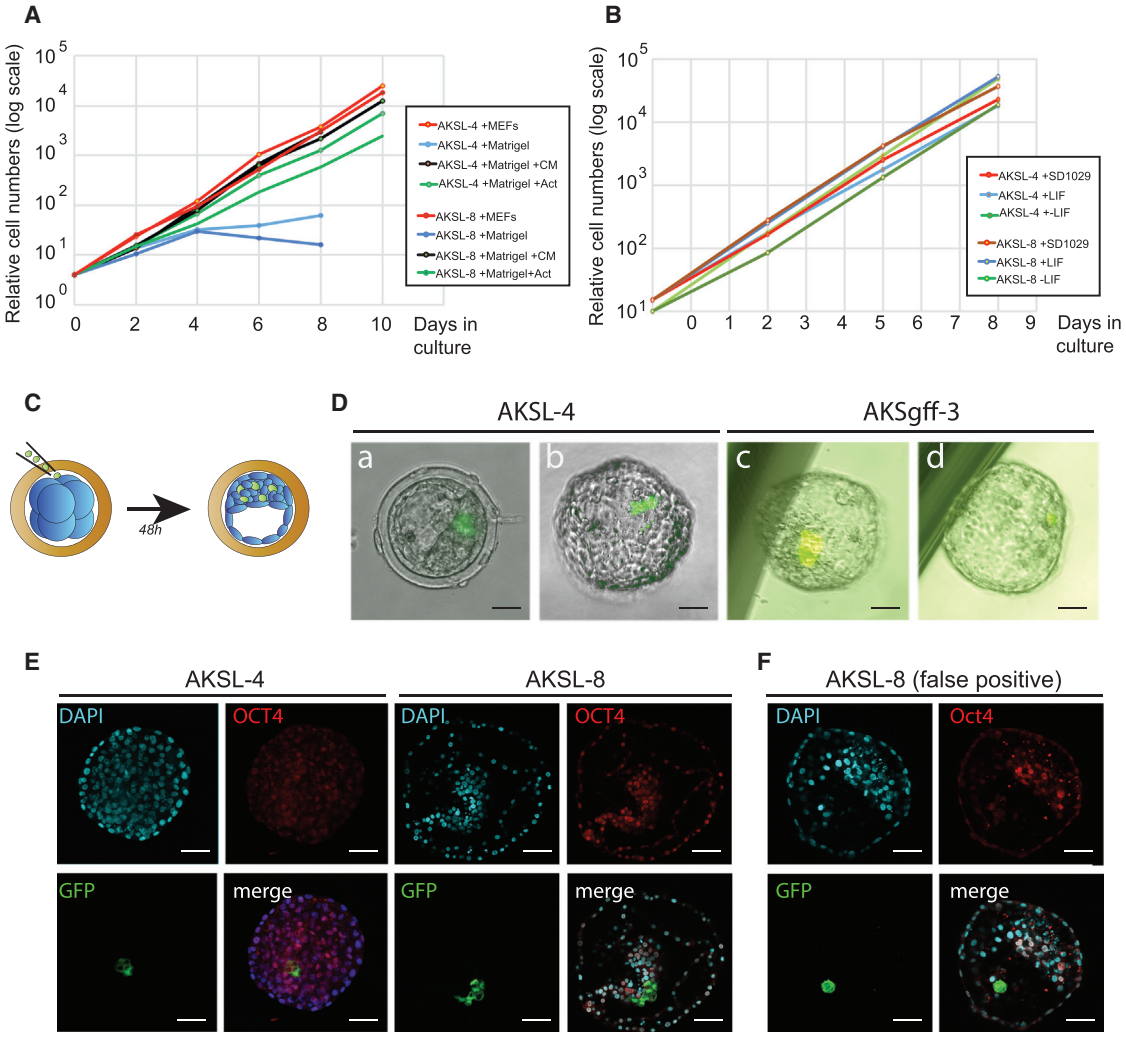

Figure 7. Embryo Colonization by AKSL and AKSgff Cells

(A) Growth curve for AKSL-4 and AKSL-8 cells after propagation for 8 days on growth-inactivated MEFs (control cells), Matrigel (with no supplementation), Matrigel with MEF-conditioned medium, and Matrigel with 5 ng/ml activin, calculated from one experiment.

(B) Growth curve for AKSL-4 and AKSL-8 cells cultivated with or without LIF and with the JAK inhibitor SD1029 calculated from one experiment.

(C) Injection of rbESCs into 8-cell stage embryos and in vitro cultured for 2–4 days.

(D) Phase-contrast and fluorescence images of (a) mid-blastocyst stage embryo (E3.5) and (b) late-blastocyst stage embryos (E5.5) resulting from the microinjection of AKSL-4 cells, and (c and d) late-blastocyst stage embryos (E5.5) resulting from the microinjection of AKSgff-3 cells. Scale bars, 50 μm.

(E) Fluorescent images of late-blastocyst stage embryos (E5.5) resulting from the microinjection of AKSL-4 and AKSL-8 cells observed by confocal microscopy (DNA staining with DAPI, blue; immunostaining for Oct4, red; immunostaining for GFP, green). Scale bars, 50 μm.

(F) Typical false-positive embryo showing one single GFP-positive cell in the blastocele. Scale bars, 50 μm.

See Figures S6 and S7.

4 days resulted in morphological differentiation (Figure S6C) and the loss of Oct4 and Nanog expression (Figure S6D). Thus, AKSL cells are dependent on activin signaling for self-renewal. Conversely, AKSL cells cultured in LIF-free medium or with the JAK inhibitor III SD-1029 displayed no morphological alteration or growth retardation and no alteration in *Oct4* and *Nanog* expression, strongly suggesting that AKSL cells are not dependent on LIF/JAK signaling for self-renewal (Figures 7B and S7).

Embryo Colonization by Rabbit ESCs

We previously reported that rbESCs derived from rabbit ICMs after partial dissociation with collagenase and culture in FGF2-supplemented medium (i.e., CKF), could not

Table 1. Colonization of Rabbit Blastocysts by AKSL-GFP and AKSgff-GFP Cells

	CKF	AKF		AKSF		AKSgff		AKSL	
Line no.	18	5	20	19	26	3	62	4	8
No. of injected embryos	87	82	84	78	82	61	56	75	71
No. of blastocysts	74	68	77	64	66	39	40	64	61
No. of blastocysts with GFP-positive cells	0	0	0	0	0	4	2	12	6
No. of blastocysts with colonized ICM	0	0	0	0	0	2	1	12	5

colonize the ICM after microinjection into rabbit embryos (Osteil et al., 2013). The capacity to colonize the ICM of the pre-implantation embryo is often viewed as a hallmark of the naive state of pluripotency. We thus asked whether the other types of cells cultured in this study had acquired this capacity. To this aim, CKF, AKF, AKSF, AKSL, and AKSgff cells were labeled with the GFP via infection with the *GAE-WPRE-CAG-GFP* lentiviral vector. In total, five to ten GFP-positive cells were injected into 4- to 8-cell-stage rabbit embryos (Figure 7C). The embryos were cultured for 4 days until they reached the late-blastocyst stage (E5.5). No cell line propagated in FGF2-supplemented medium could colonize the ICM. Conversely, 3 of 117 E4 blastocysts exhibited colonization of the ICM by GFP-positive cells after injection of AKSgff cells, and 17 of 146 embryos exhibited colonization after AKSL cell injection (Table 1; Figures 7D and 7E). Therefore, the AKSL cells display an increased competency for embryo colonization compared with the AKSgff cells. Note that embryos with GFP-positive cells outside the embryonic disk (Figure 7F) were not considered in the calculation of colonization efficiency. Thus, some cells within the populations of AKSL and AKSgff cells had the capacity to colonize the rabbit embryo and participate in ICM formation.

DISCUSSION

Until now, rabbit ESC lines were derived from ICMs using culture conditions applied to the derivation of human and non-human primate ESC lines, including partial dissociation with collagenase II and culture medium supplemented with KOSR and FGF2 (Honda et al., 2009; Osteil et al., 2013; Wang et al., 2006). These culture conditions produced rbESC lines exhibiting molecular and functional features associated with primed pluripotency, including the failure to colonize the rabbit epiblast (Osteil et al., 2013). Here, we found that ESC lines can be derived from rabbit ICMs after single-cell dissociation with Accutase in culture medium lacking FGF2 and supplemented with FCS. The resulting lines and the conventional rbESC lines derived in CKF conditions exhibited striking differences. First, the transcriptome of the AKF, AKSF, AKSL, and AKSgff lines is closer to that of the rabbit ICM and epiblast, suggesting that single-cell dissociation, withdrawal of FGF2, and medium supplementation with FCS help rbESCs retain the gene expression profile of the original ICM/epiblast stem cells. Second, their cell cycle is altered. Unlike ESC lines generated in mice, monkeys, and humans (Aladjem et al., 1998; Filipczyk et al., 2007; Fluckiger et al., 2006; Momcilovic et al., 2009), conventional rbESCs exhibit G_1 growth arrest after DNA damage, revealing the presence of a checkpoint before entry into S phase similar to somatic cells (Osteil et al., 2013). All rbESC lines derived using single-cell dissociation and FCS supplementation exhibited a shorter G_1 phase and lacked the G_1 checkpoint, similar to rodent and primate PSCs. Third, rbESCs derived by single-cell dissociation with Accutase in culture medium supplemented with FCS acquired the capacity to colonize the epiblast of the rabbit blastocysts. These observations strongly suggest that single-cell dissociation, withdrawal of FGF2, and medium supplementation with FCS help ESCs to retain the biological characteristics of the original ICM/epiblast cells. It must be stressed that AKSL and AKSgff cells do not exhibit the same gene expression profiles as the ICM/epiblast, suggesting that the culture conditions for capturing the original state of pluripotency need to be further refined.

An important issue is whether rbESC lines derived using single-cell dissociation and FCS supplementation in the absence of FGF2 acquired the characteristics of naive-like pluripotency, as defined in mice. First, rbESCs exhibited embryo colonization competency after injection into 8-cell-stage rabbit embryos, a functional characteristic of naive PSCs. The efficiency is low, which might be explained by the cell heterogeneity. Indeed, single-cell transcriptome analysis revealed that 21% of AKSL cells and 28% of AKSgff cells co-express the markers of naive pluripotency *Esrrb*, *Tfcp2l1*, *Klf4*, *Tbx3*, and *Rex1* (*Zfp42*). Assuming that only these cells are endowed with embryo colonization competence, the average number of competent cells injected into 8-cell-stage embryos ranged from 1 to 2.8. Second, the transcriptome analysis supports a shift toward a more immature pluripotency. Similar to primed PSCs, rbESC lines derived and propagated in conventional conditions (i.e., CKF) express lineage markers at higher levels. Conversely, rbESCs derived and propagated by single-cell dissociation in the absence of FGF2 express genes and miRNAs associated with naive pluripotency in mice (i.e., *Gdf3*, *Tbx3*, *Prdm14*, and *Rex1* [*Zfp42*]) and the *ocu-miR290* cluster (Bao et al., 2009; Chen et al., 2015; Parchem

et al., 2014; Tang et al., 2010; Tesar et al., 2007) at higher levels. These observations strongly suggest that conditions for deriving and expanding rbESCs including single-cell dissociation with Accutase, FCS supplementation, and a lack of FGF2 coax rbESCs toward a more immature phenotype. However, these rbESCs do not exhibit all of the characteristics of mouse ESCs, suggesting that they self-renew in an intermediate state between primed and naive pluripotency. Particularly, they rely on activin signaling for self-renewal, similar to intermediate epiblast stem cells in mice (Chang and Li, 2013) and human ESCs after reprogramming to naive-like pluripotency (Theunissen et al., 2014). We also failed to derive rbESC lines using culture conditions that incorporate MEK and GSK3 inhibitors (2i condition), a hallmark of naive-state pluripotency in rodents (Silva et al., 2008; Ying et al., 2008) and humans (Chen et al., 2015; Takashima et al., 2014; Theunissen et al., 2014). This latter observation raises the question of whether resistance to MEK inhibition should be incorporated into the definition of naive pluripotency in rabbits.

Whether LIF contributes to differentiation inhibition in rabbit PSCs is unclear. LIF and FGF2 cooperatively support self-renewal in ESCs derived from parthenogenotes and propagated in feeder-free conditions, but the effect of LIF is modest (Hsieh et al., 2011). In this study, AKSL and AKSgff cell lines exhibited similar growth parameters, cell-cycle features, and transcriptomes. Moreover, neither withdrawal of LIF nor JAK inhibition resulted in observable differentiation, suggesting that LIF/JAK signaling in the presence of feeders is dispensable for self-renewal in rbESCs. However, the AKSL line was more efficient at colonizing the epiblast of the rabbit embryo, suggesting a more immature phenotype.

EXPERIMENTAL PROCEDURES

All the procedures used in the study followed the national and European regulations concerning animal experiments, and were approved by the authorized national and veterinary agencies. A detailed description of the procedures is provided in Supplemental Experimental Procedures.

Embryo Production and ICM Culture

Morula-stage embryos were flushed from explanted oviducts and cultured for 24 hr in RDH medium until they reached the mid-blastocyst stage. The mucin coat and zona pellucida were removed after treatment with pronase, and the trophoblast was removed by mechanical dissociation. ICMs were subsequently transferred to 4-well plates on mitomycin C-treated MEFs. After 6–7 days, outgrowths were cut into small pieces and placed in a new well (passage 1). After 3–4 days, the newly formed colonies were dissociated into either small clumps using collagenase II followed by manual picking or single cells using Accutase (passage 2) and transferred onto fresh feeder cells. All subsequent passages were performed by enzymatic dissociation after treating colonies with collagenase II and manual picking or with Accutase.

Isolation of ICM and Epiblast for Transcriptome Study

Mid-blastocysts (E4) were collected 96 hr after artificial insemination and incubated in 5 mg/mL pronase at room temperature to remove the zona pellucida and mucin coat. The ICM was separated from the trophectoderm by immunosurgery followed by gentle pipetting with a glass pipette. For preparation of epiblasts, expanded blastocysts (E6) were collected 147 hr after artificial insemination and placed in FHM medium. The zona pellucida was mechanically removed. The embryo was opened and flattened on a plastic dish to expose the embryoblast. The hypoblast was first dissociated by careful scratching with a glass needle, and the epiblast was then separated from the trophoblast with a microscalpel.

Cell Microinjection and Immunolabeling of Embryos and Cells

ESCs were dissociated into single-cell suspensions, and 5–10 cells were microinjected under the zona pellucida of 6- to 8-cell stage rabbit embryos (E1.5). After 48 hr of in vitro culture in RDH medium, blastocyst stage embryos (E3.5) were treated with pronase to digest the mucus coat. They were further cultured in RDH medium for 48 hr until they reached the late-blastocyst stage (E5.5) prior to immunostaining with AF488-conjugated rabbit anti-GFP antibody or Anti-Oct4 antibody (Santa Cruz biotechnology, sc-9081). Cells were immunolabeled with Alexa Fluor 647-conjugated SSEA1 (Santa Cruz, sc-21702) and Alexa Fluor 647-conjugated SSEA4 (Santa Cruz, sc-21704) antibodies.

Real-Time and Single-Cell Gene Expression qRT-PCR

Real-time PCR was performed using the StepOnePlus real-time PCR system and Fast SYBR Green Master Mix (Applied Biosystems). Expression of the target genes was normalized to those of the rabbit TATA-box binding protein (*Tbp*) and *Gapdh* genes. For single-cell qPCR, cells were dissociated using Accutase. Single cells were captured on the C1 Array IFC (10–17 μm) and subjected to reverse transcription and specific target amplification using components from the Cells-to-Ct kit (Ambion) and C1 Single-Cell Auto Prep Modules kit (Fluidigm). These pre-amplified products were subsequently analyzed with Universal PCR TaqMan Master Mix (Applied Biosystems) and coupled with a DNA Binding Dye Sample Loading Reagent (Fluidigm) and Evagreen (Biotium 31000) in 96.96 Dynamic Arrays on a BioMark system.

miRNA Quantification

Mature miRNA quantification was performed via a two-step protocol including reverse transcription with miRNA-specific primers using a TaqMan MicroRNA Reverse Transcription kit, followed by real-time qPCR with TaqMan MicroRNA Assays. Expression of the target miRNAs was normalized to the housekeeping miRNAs *ocu-miR-191* and *ocu-miR-423*.

ACCESSION NUMBERS

The accession number for the microarray data reported in this paper is GEO: GSE79195.

SUPPLEMENTAL INFORMATION

Supplemental Information includes Supplemental Experimental Procedures, seven figures, and one table and can be found with this article online at http://dx.doi.org/10.1016/j.stemcr.2016.07.022.

AUTHOR CONTRIBUTIONS

P.O.: conception and design, collection and/or assembly of data, data analysis and interpretation, and manuscript writing; A.M., C.S., M.A., Y.T., C.A., B.S.-P., J.L., C.G., A.R., C.D., H.B., and N.M.-B.: collection and/or assembly of data; T.J.: provision of study material and collection and/or assembly of data; L.J.: statistics and bioinformatics; H.A.: data analysis and interpretation; E.G.: conception and design, and data analysis and interpretation; V.D. and M.A.: conception and design, data analysis and interpretation, and manuscript writing; P.S.: conception and design, data analysis and interpretation, manuscript writing, and financial support.

ACKNOWLEDGMENTS

We thank Anaïs Vitorino Carvalho for microarray probe annotation. This study was supported by research grants from the Agence Nationale de la Recherche (ANR; projects PLURABBIT no. PCS-09-GENM-08 and ORYCTOGENE no. ANR-12-RPIB-0013), European Cooperation in Science and Technology (COST) Action (Rabbit Genome Biology [RGB]-Net no. TD1101), HyPharm, Région Rhône-Alpes (ADR CIBLE 2010 project no. R10065CC to Y.T.), Infrastructure Nationale en Biologie et Santé INGESTEM (ANR-11-INBS-0009), Infrastructure Nationale en Biologie et Santé CRB-Anim (ANR-11-INBS-0003), IHU-B CESAME (ANR-10-IHUB-003), LabEx DEVweCAN (ANR-10-LABX-0061), LabEx CORTEX (ANR-11-LABX-0042) of the University of Lyon within the program Investissements d'Avenir (ANR-11-IDEX-0007), and Fondation pour la Recherche Médicale (FRM SPE20140129375) to P.O. The authors would like to thank Enago (www.enago.com) for the English language review.

Received: March 17, 2016
Revised: July 27, 2016
Accepted: July 28, 2016
Published: September 1, 2016

REFERENCES

Aladjem, M.I., Spike, B.T., Rodewald, L.W., Hope, T.J., Klemm, M., Jaenisch, R., and Wahl, G.M. (1998). ES cells do not activate p53-dependent stress responses and undergo p53-independent apoptosis in response to DNA damage. Curr. Biol. *8*, 145–155.

Bao, S., Tang, F., Li, X., Hayashi, K., Gillich, A., Lao, K., and Surani, M.A. (2009). Epigenetic reversion of post-implantation epiblast to pluripotent embryonic stem cells. Nature *461*, 1292–1295.

Bourillot, P.Y., Aksoy, I., Schreiber, V., Wianny, F., Schulz, H., Hummel, O., Hubner, N., and Savatier, P. (2009). Novel STAT3 target genes exert distinct roles in the inhibition of mesoderm and endoderm differentiation in cooperation with Nanog. Stem Cells *27*, 1760–1771.

Brons, I.G., Smithers, L.E., Trotter, M.W., Rugg-Gunn, P., Sun, B., Chuva de Sousa Lopes, S.M., Howlett, S.K., Clarkson, A., Ahrlund-Richter, L., Pedersen, R.A., et al. (2007). Derivation of pluripotent epiblast stem cells from mammalian embryos. Nature *448*, 191–195.

Chang, K.H., and Li, M. (2013). Clonal isolation of an intermediate pluripotent stem cell state. Stem Cells *31*, 918–927.

Chen, H., Aksoy, I., Gonnot, F., Osteil, P., Aubry, M., Hamela, C., Rognard, C., Hochard, A., Voisin, S., Fontaine, E., et al. (2015). Reinforcement of STAT3 activity reprogrammes human embryonic stem cells to naïve-like pluripotency. Nat. Commun. *6*, 7095–7111.

Filipczyk, A., Laslett, A.L., Mummery, C., and Pera, M. (2007). Differentiation is coupled to changes in the cell cycle regulatory apparatus of human embryonic stem cells. Stem Cell Res. *1*, 45–60.

Fluckiger, A.C., Marcy, G., Marchand, M., Negre, D., Cosset, F.L., Mitalipov, S., Wolf, D., Savatier, P., and Dehay, C. (2006). Cell cycle features of primate embryonic stem cells. Stem Cells *24*, 547–556.

Honda, A., Hirose, M., Inoue, K., Ogonuki, N., Miki, H., Shimozawa, N., Hatori, M., Shimizu, N., Murata, T., Hirose, M., et al. (2008). Stable embryonic stem cell lines in rabbits: potential small animal models for human research. Reprod. Biomed. Online *17*, 706–715.

Honda, A., Hirose, M., and Ogura, A. (2009). Basic FGF and Activin/Nodal but not LIF signaling sustain undifferentiated status of rabbit embryonic stem cells. Exp. Cell. Res. *315*, 2033–2042.

Hsieh, Y.C., Intawicha, P., Lee, K.H., Chiu, Y.T., Lo, N.W., and Ju, J.C. (2011). LIF and FGF cooperatively support stemness of rabbit embryonic stem cells derived from parthenogenetically activated embryos. Cell Reprogram *13*, 241–255.

Intawicha, P., Ou, Y.W., Lo, N.W., Zhang, S.C., Chen, Y.Z., Lin, T.A., Su, H.L., Guu, H.F., Chen, M.J., Lee, K.H., et al. (2009). Characterization of embryonic stem cell lines derived from New Zealand white rabbit embryos. Cloning Stem Cells *11*, 27–38.

Jacquier, V., Estelle, J., Schmaltz-Panneau, B., Lecardonnel, J., Moroldo, M., Lemonnier, G., Turner-Maier, J., Duranthon, V., Oswald, I.P., Gidenne, T., et al. (2015). Genome-wide immunity studies in the rabbit: transcriptome variations in peripheral blood mononuclear cells after in vitro stimulation by LPS or PMA-ionomycin. BMC Genomics *16*, 26.

Manor, Y.S., Massarwa, R., and Hanna, J.H. (2015). Establishing the human naive pluripotent state. Curr. Opin. Genet. Dev. *34*, 35–45.

Maraghechi, P., Hiripi, L., Toth, G., Bontovics, B., Bosze, Z., and Gocza, E. (2013). Discovery of pluripotency associated microRNAs in rabbit preimplantation embryos and embryonic stem-like cells. Reproduction *145*, 421–437.

Momcilovic, O., Choi, S., Varum, S., Bakkenist, C., Schatten, G., and Navara, C. (2009). Ionizing radiation induces atm dependent checkpoint signaling and G(2) but not G(1) cell cycle arrest in pluripotent human embryonic stem cells. Stem Cells *27*, 1822–1835.

Nichols, J., and Smith, A. (2009). Naive and primed pluripotent states. Cell Stem Cell *4*, 487–492.

Osteil, P., Tapponnier, Y., Markossian, S., Godet, M., Schmaltz-Panneau, B., Jouneau, L., Cabau, C., Joly, T., Blachere, T., Gocza, E., et al. (2013). Induced pluripotent stem cells derived from rabbits

exhibit some characteristics of naive pluripotency. Biol. Open *2*, 613–628.

Parchem, R.J., Ye, J., Judson, R.L., Larussa, M.F., Krishnakumar, R., Blelloch, A., Oldham, M.C., and Blelloch, R. (2014). Two miRNA clusters reveal alternative paths in late-stage reprogramming. Cell Stem Cell *14*, 617–631.

Püschel, B., and Viebahn, C. (2010). Rabbit mating and embryo isolation. Cold Spring Harb. Protoc. *2*, 500–508.

Schmaltz-Panneau, B., Jouneau, L., Osteil, P., Tapponnier, Y., Afanassieff, M., Moroldo, M., Jouneau, A., Daniel, N., Archilla, C., Savatier, P., et al. (2014). Contrasting transcriptome landscapes of rabbit pluripotent stem cells in vitro and in vivo. Anim. Reprod. Sci. *149*, 67–79.

Silva, J., Barrandon, O., Nichols, J., Kawaguchi, J., Theunissen, T.W., and Smith, A. (2008). Promotion of reprogramming to ground state pluripotency by signal inhibition. PLoS Biol. *6*, e253.

Tachibana, M., Sparman, M., Ramsey, C., Ma, H., Lee, H.S., Penedo, M.C., and Mitalipov, S. (2012). Generation of chimeric rhesus monkeys. Cell *148*, 285–295.

Takashima, Y., Guo, G., Loos, R., Nichols, J., Ficz, G., Krueger, F., Oxley, D., Santos, F., Clarke, J., Mansfield, W., et al. (2014). Resetting transcription factor control circuitry toward ground-state pluripotency in human. Cell *158*, 1254–1269.

Tancos, Z., Nemes, C., Polgar, Z., Gocza, E., Daniel, N., Stout, T.A., Maraghechi, P., Pirity, M.K., Osteil, P., Tapponnier, Y., et al. (2012). Generation of rabbit pluripotent stem cell lines. Theriogenology *78*, 1774–1786.

Tang, F., Barbacioru, C., Bao, S., Lee, C., Nordman, E., Wang, X., Lao, K., and Surani, M.A. (2010). Tracing the derivation of embryonic stem cells from the inner cell mass by single-cell RNA-seq analysis. Cell Stem Cell *6*, 468–478.

Tesar, P.J., Chenoweth, J.G., Brook, F.A., Davies, T.J., Evans, E.P., Mack, D.L., Gardner, R.L., and McKay, R.D. (2007). New cell lines from mouse epiblast share defining features with human embryonic stem cells. Nature *448*, 196–199.

Theunissen, T.W., Powell, B.E., Wang, H., Mitalipova, M., Faddah, D.A., Reddy, J., Fan, Z.P., Maetzel, D., Ganz, K., Shi, L., et al. (2014). Systematic identification of culture conditions for induction and maintenance of naive human pluripotency. Cell Stem Cell *15*, 471–487.

Thevenot, E.A., Roux, A., Xu, Y., Ezan, E., and Junot, C. (2015). Analysis of the human adult urinary metabolome variations with age, body mass index and gender by implementing a comprehensive workflow for univariate and OPLS statistical analyses. J. Proteome Res. *14*, 3322–3335.

Wang, S., Tang, X., Niu, Y., Chen, H., Li, B., Li, T., Zhang, X., Hu, Z., and Ji, W. (2006). Generation and characterization of rabbit embryonic stem cells. Stem Cells *25*, 481–489.

Wang, S., Shen, Y., Yuan, X., Chen, K., Guo, X., Chen, Y., Niu, Y., Li, J., Xu, R.H., Yan, X., et al. (2008). Dissecting signaling pathways that govern self-renewal of rabbit embryonic stem cells. J. Biol. Chem. *19*, 35929–35940.

Ying, Q.L., Wray, J., Nichols, J., Batlle-Morera, L., Doble, B., Woodgett, J., Cohen, P., and Smith, A. (2008). The ground state of embryonic stem cell self-renewal. Nature *453*, 519–523.